APL Photonics

RESEARCH ARTICLE | DECEMBER 12 2023

Sideband injection locking in microresonator frequency combs

Special Collection: State-of-the-Art and Future Directions in Optical Frequency Comb Sources, Enabling Technologies, and Applications

Thibault Wildi ; Alexander Ulanov ; Nicolas Englebert ; Thibault Voumard ; Tobias Herr

APL Photonics 8, 120801 (2023)
https://doi.org/10.1063/5.0170224

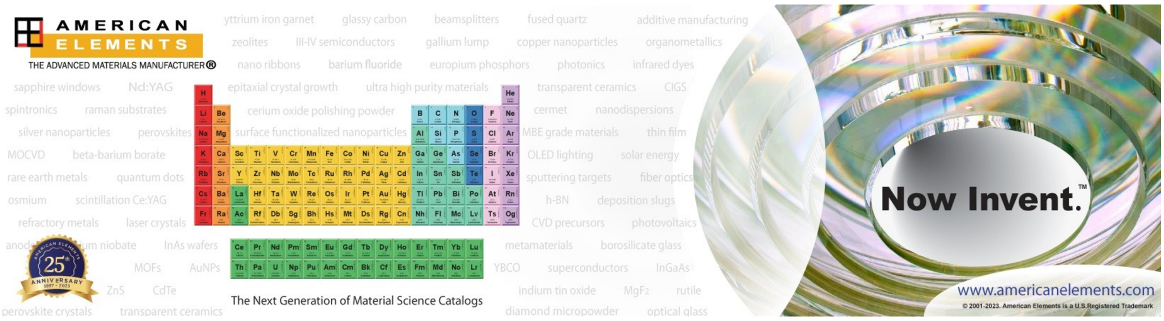

APL Photonics | ARTICLE | pubs.aip.org/aip/app

Sideband injection locking in microresonator frequency combs

Cite as: APL Photon. 8, 120801 (2023); doi: 10.1063/5.0170224
Submitted: 1 August 2023 • Accepted: 8 November 2023 •
Published Online: 12 December 2023

View Online | Export Citation | CrossMark

Thibault Wildi,[1] Alexander Ulanov,[1] Nicolas Englebert,[2] Thibault Voumard,[1] and Tobias Herr[1,3,a)]

AFFILIATIONS

[1] Deutsches Elektronen-Synchrotron DESY, Notkestr. 85, 22607 Hamburg, Germany
[2] OPERA-Photonics, Université libre de Bruxelles (U.L.B.), 50 Avenue F. D. Roosevelt, CP 194/5, B-1050 Brussels, Belgium
[3] Physics Department, Universität Hamburg UHH, Luruper Chaussee 149, 22761 Hamburg, Germany

Note: This paper is part of the APL Photonics Special Topic on State-of-the-Art and Future Directions in Optical Frequency Comb Sources, Enabling Technologies, and Applications.
[a)] **Author to whom correspondence should be addressed:** tobias.herr@desy.de

ABSTRACT

Frequency combs from continuous-wave-driven Kerr-nonlinear microresonators have evolved into a key photonic technology with applications from optical communication to precision spectroscopy. Essential to many of these applications is the control of the comb's defining parameters, i.e., carrier-envelope offset frequency and repetition rate. An elegant and all-optical approach to controlling both degrees of freedom is the suitable injection of a secondary continuous-wave laser into the resonator onto which one of the comb lines locks. Here, we experimentally study such *sideband injection locking* in microresonator soliton combs across a wide optical bandwidth and derive analytic scaling laws for the locking range and repetition rate control. As an application example, we demonstrate optical frequency division and repetition rate phase-noise reduction to three orders of magnitude below the noise of a free-running system. The presented results can guide the design of sideband injection-locked, parametrically generated frequency combs with opportunities for low-noise microwave generation, compact optical clocks with simplified locking schemes, and, more generally, all-optically stabilized frequency combs from Kerr-nonlinear resonators.

I. INTRODUCTION

Continuous-wave (CW) coherently driven Kerr-nonlinear resonators can create temporally structured waveforms that circulate stably without changing their temporal or spectral intensity profile. The out-coupled optical signal is periodic with the resonator roundtrip time T_{rep} and corresponds to an optical frequency comb,[1–5] i.e., a large set of laser frequencies spaced by the repetition rate $f_{\mathrm{rep}} = T_{\mathrm{rep}}^{-1}$. One important class of such stable waveforms are CW-driven dissipative Kerr-solitons (DKSs), which have been observed in fiber-loops,[6] traveling- and standing-wave microresonators,[7,8] and free-space cavities.[9] In microresonators, these soliton microcombs[10] provide access to low-noise frequency combs with ultra-high repetition rates up to THz frequencies, enabling novel applications in diverse fields, including optical communication,[11,12] ranging,[13–15] astronomy,[16,17] spectroscopy,[18] microwave photonics,[19,20] and all-optical convolutional neural networks.[21]

In a CW-driven microresonator, the comb's frequency components are defined by $f_\mu = f_{\mathrm{p}} + \mu f_{\mathrm{rep}}$, where f_{p} denotes the frequency of the central comb line and μ is the index of the comb line with respect to the central line (μ is also used to index the resonances supporting the respective comb lines). For many applications,[4,5] it is essential to control both degrees of freedom in the generated frequency comb spectra, i.e., the repetition rate f_{rep} and the central frequency f_{p} (which together define the comb's carrier-envelope offset frequency). Conveniently, for Kerr-resonator-based combs, f_{p} is defined by the pump laser frequency $f_{\mathrm{p}} = \omega_{\mathrm{p}}/(2\pi)$. However, the repetition rate f_{rep} depends on the resonator and is subject to fundamental quantum mechanical as well as environmental fluctuations.

A particularly attractive and all-optical approach to controlling f_{rep} is the injection of a secondary CW laser of frequency ω' into the resonator, demonstrated numerically[22] and experimentally.[23] If ω' is sufficiently close to one of the free-running comb lines (sidebands) $f_\mu \approx \omega'/(2\pi)$, i.e., within *locking range*, the comb will lock onto the secondary laser so that $f_\mu \to \omega'/(2\pi)$. The repetition rate is then $f_{rep} = (\omega_p - \omega')/(2\pi\mu')$, with μ' denoting the index of the closest resonance to which the secondary laser couples; cf. Fig. 1(a). This frequency division[24] of the frequency interval defined by the two CW lasers (as well as their relative frequency noise) by the integer μ' can give rise to a low-noise repetition rate f_{rep}. In previous work, sideband injection locking has been leveraged across a large range of photonic systems, including for parametric seeding,[25,26] dichromatic pumping,[27] optical trapping,[22,28,29] synchronization of solitonic and non-solitonic combs,[30,31] soliton crystals,[23] soliton time crystals,[32] multi-color solitons,[33] and optical clockworks by injection into a DKS dispersive wave.[34] Related dynamics also govern the self-synchronization of comb states,[35,36] the binding between solitons,[37] modified soliton dynamics in the presence of Raman effect[38] and avoided mode-crossings,[39] as well as the respective interplay between co-propagating[40] and counter-propagating solitons[41–43] and multi-soliton state-switching.[44] Moreover, sideband injection locking is related to modulated and pulsed driving for broadband stabilized combs,[17,45,46] as well as spectral purification and nonlinear filtering of microwave signals[47,48] via DKSs. Despite the significance of sideband injection locking, a broadband characterization and quantitative understanding of its dependence on the injecting laser are lacking, making the design and implementation of such systems challenging.

In this work, we study the dynamics of sideband injection locking with DKS combs. Our approach leverages high-resolution coherent spectroscopy of the microresonator under DKS operation, enabling precise mapping of locking dynamics across a large set of comb modes, including both the central region and the wing of the comb. We derive the sideband injection locking range's dependence on experimentally accessible parameters and find excellent agreement with the experimental observation and numerical simulation. Specifically, this includes the square dependence on the mode number, the square-root dependence on injection laser and DKS spectral power, as well as the associated spectral shifts.

In addition, we experimentally demonstrate the optical frequency division and repetition rate phase-noise reduction in a DKS state to three orders of magnitude below the noise of a free-running system.

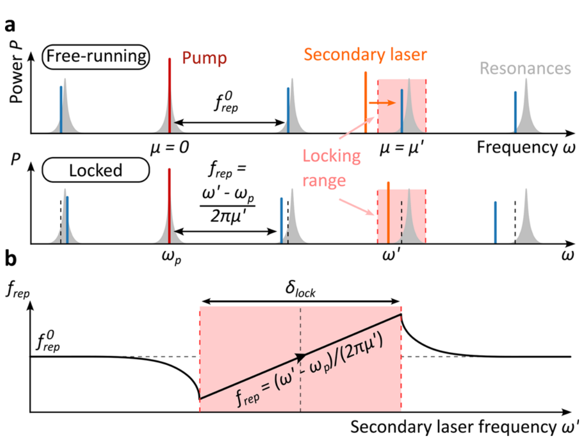

FIG. 1. Principles of sideband injection locking. (a) In a free-running comb, the central comb line is defined by the pump laser around which equidistant comb lines, spaced by the free-running repetition rate f^0_{rep}, are formed. If a secondary injection laser of frequency ω' is brought close to one of the comb lines (within injection locking range), then the comb locks to the injecting laser, modifying the repetition rate as indicated. (b) Outside the locking range, $f_{rep} = f^0_{rep}$ is unaffected by the secondary laser. Inside the locking range, it follows a characteristic tuning behavior with a linear dependence on the injecting laser frequency ω'.

II. RESULTS

To first explore the sideband injection locking dynamics experimentally, we generate a single DKS state in a silicon nitride ring-microresonator. In the fundamental TE modes, the resonator is characterized by a quality factor of $Q \approx 2 \times 10^6$ [linewidth $\kappa/(2\pi) \approx 100$ MHz] and a free-spectral range (FSR) of $D_1/(2\pi) = 300$ GHz and exhibits an anomalous group velocity dispersion $D_2/(2\pi) = 9.7$ MHz so that the resonance frequencies are well-described by $\omega_\mu = \omega_0 + \mu D_1 + \mu^2 \frac{D_2}{2}$ ($1.6 \times 0.8\,\mu$m^2 cross section, 76 μm radius). To achieve a deterministic single soliton initiation, the microresonator's inner perimeter is weakly corrugated.[49,50] The resonator is critically coupled and driven by a CW pump laser (~300 kHz linewidth) with an on-chip power of 200 mW at 1557 nm [pump frequency $\omega_p/(2\pi) = 192.5$ THz].[7] The generated DKS has a 3 dB bandwidth of ~5.2 THz [cf. Fig. 2(a)] corresponding to a bandwidth limited pulse of ~60 fs duration. The soliton spectrum closely follows a sech^2 envelope and is free of dispersive waves or avoided mode crossings. The spectral center of the soliton does not coincide with the pump laser but is slightly shifted toward longer wavelengths due to the Raman self-frequency shift.[51,52]

A secondary CW laser (~300 kHz linewidth), tunable both in power and in frequency (and not phase-locked in any way to the first CW laser), is then combined with the pump laser upstream of the microresonator and scanned across the μ'th sideband of the soliton microcomb, as illustrated in Fig. 2(a). The spectrogram of the repetition rate signal recorded during this process is shown in Fig. 2(b), for $\mu' = -13$, and exhibits the canonical signature of locking oscillators[53] (see Sec. II of the supplementary material for details on the measurement of f_{rep}). Specifically, the soliton repetition rate f_{rep} is observed to depend linearly on the auxiliary laser frequency ω' over a locking range δ_{lock} following $f_{rep} = \frac{1}{2\pi}\frac{\omega_p - \omega'}{\mu'}$. Within δ_{lock}, the soliton comb latches onto the auxiliary laser such that the frequency of the comb line with index μ' is equal to the secondary laser frequency. The locking behavior is found to be symmetric with respect to the scanning direction, and no hysteresis is observed. Figure 2(c) shows the optical spectra of two sideband injection-locked DKS states, with the secondary laser positioned close to the respective boundaries of the locking range. A marked shift of the spectrum of 860 GHz is visible when going from one state to the other. As we discuss below and in Sec. III B of the supplementary material, the spectral shift in the presence of non-zero group velocity dispersion modifies the soliton's group velocity and provides a mechanism for the DKS to adapt to the repetition rate imposed by the driving lasers.

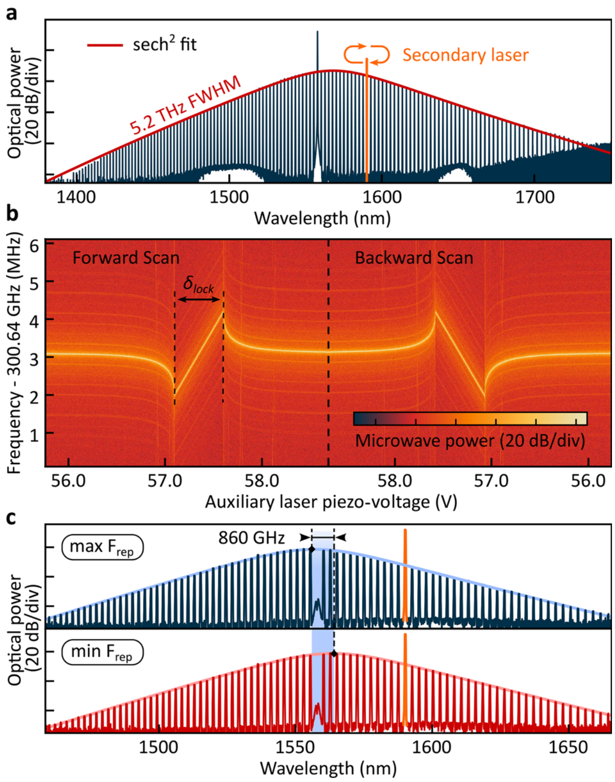

FIG. 2. Soliton sideband injection locking. (a) Single DKS comb spectrum, following a *sech*^{2} envelope, with a full-width-at-half-maximum (FWHM) of 5.2 THz, corresponding to a ~60 fs pulse. The secondary laser is introduced in the spectral wing of the soliton and scanned across the μ'th sideband. (b) Repetition rate beatnote observed while the secondary laser is scanned across the μ'th sideband. The locking bandwidth corresponds to the region of linear evolution of the repetition rate beatnote. (c) Spectra of two sideband injection-locked DKS states from either end of the locking range, exhibiting a differential spectral shift of 860 GHz. Note that a filter blocks the central pump component ω_p.

Having identified characteristic features of sideband injection locking in our system, we systematically study the injection locking range and its dependence on the mode number μ' to which the secondary laser is coupled. To this end, a frequency comb calibrated scan[54] of the secondary laser's frequency ω' across many DKS lines is performed. The power transmitted through the resonator coupling waveguide is simultaneously recorded. It contains the ω'-dependent transmission of the secondary laser as well as the laser's heterodyne mixing signal with the DKS comb, which permits retrieving the locking range δ_{lock}.

Figure 3(a) shows an example of the recorded transmission signal, where the scanning laser's frequency ω' is in the vicinity of the comb line with index $\mu' = -3$. When the laser frequency ω' is sufficiently close to the DKS comb line, the heterodyne oscillations (blue trace) can be sampled; when ω' is within the locking range δ_{lock}, the heterodyne oscillations vanish, and a linear slope is visible, indicating the changing phase between the comb line and the secondary laser across the injection locking range. In addition to the heterodyne signal between the comb line and the laser, a characteristic resonance feature, the so-called C-resonance,[55,56] representing (approximately) the resonance frequency ω_μ is observed.

The set of equivalent traces for all comb lines μ' in the range of the secondary (scanning) laser is presented in Fig. 3(b) as a horizontal stack. For plotting these segments on a joint vertical axis, $\omega_p + \mu' D_1$ has been subtracted from ω'. In this representation, the parabolic curve [blue line in Fig. 3(b)] connecting the C-resonances signifies the anomalous dispersion of the resonator modes ω_μ. In contrast, the equidistant comb lines form a straight feature (gray highlight), of which a magnified view is presented in Fig. 3(c). Due to the Raman self-frequency shift, the free-running repetition rate of the DKS comb f^0_{rep} is smaller than the cavity's FSR $D_1/(2\pi)$, resulting in the negative tilt of the line. Here, to obtain a horizontal arrangement of the features, $\omega_p + \mu' 2\pi f^0_{\text{rep}}$ has been subtracted from ω'. The locking range δ_{lock} corresponds to the vertical extent of the characteristic locking feature shown in Fig. 3(c). Its value is plotted as a function of the mode number in Fig. 3(d), revealing a strong mode number dependence of the locking range with local maxima (almost) symmetrically on either side of the central mode. The asymmetry in the locking range with respect to $\mu' = 0$ (with a larger locking range observed for negative values of μ') coincides with the Raman self-frequency shift of the soliton spectrum (a higher spectral intensity for negative μ). Next, we keep μ' fixed and measure the dependence of δ_{lock} on the power of the injecting laser P'. As shown in Fig. 3(e), we observe an almost perfect square-root scaling $\delta_{\text{lock}} \propto \sqrt{P'}$, revealing the proportionality of the locking range to the strength of the injected field.

The observed scaling of the locking range may be understood in both the time and frequency domains. In the time domain, the beating between the two driving lasers creates a modulated background field inside the resonator, forming an optical lattice trap for DKS pulses.[22,28] Here, to derive the injection locking range δ_{lock}, we extend the approach proposed by Taheri *et al.*,[26] which is based on the momentum $p = \sum_\mu \mu |a_\mu|^2 = \bar{\mu} \sum_\mu |a_\mu|^2$ of the waveform (in a co-moving frame), where a_μ is the complex field amplitude in the mode with index μ, normalized such that $|a_\mu|^2$ scales with the photon number, and $\bar{\mu}$ represents the *photonic center of mass* in mode number space. As shown in Sec. III C of the supplementary material, the secondary driving laser modifies the waveform's momentum and, thereby, its propagation speed and repetition rate. For the locking range of the secondary laser, we find

$$\delta_{\text{lock}} = \frac{2}{\pi} \mu'^2 \eta D_2 \frac{\sqrt{P' P_{\mu'}}}{\sum_\mu P_\mu} \frac{\omega_p}{\omega_{\mu'}}, \tag{1}$$

and for the repetition rate tuning range,

$$\delta f_{\text{rep}} = \delta_{\text{lock}} / |\mu'|, \tag{2}$$

where η is the coupling ratio and P_μ refers to the spectral power levels of the comb lines with index μ measured outside the resonator. The spectral shift of the spectrum in units of mode number μ is $2\pi \delta f_{\text{rep}} / D_2$. In Sec. I of the supplementary material, we recast Eq. (2) in terms of the injection ratio $\text{IR} = P'/P_{\mu'}$ to enable comparison with CW laser injection locking.[57] The results in Eqs. (1) and (2) may also be obtained in a frequency domain picture (see Sec. III D of the supplementary material), realizing that the waveform's

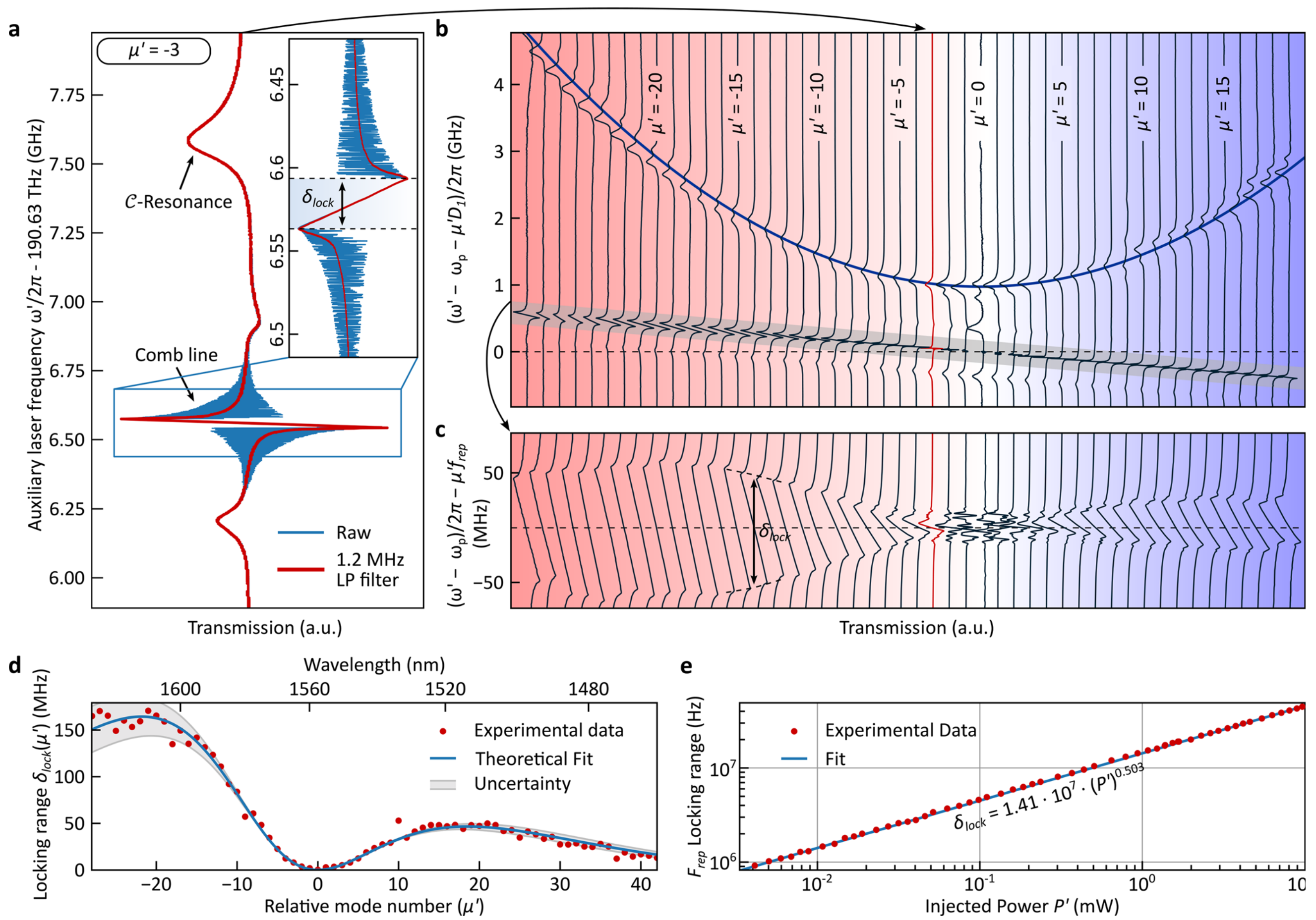

FIG. 3. DKS sideband injection locking dynamics. (a) Transmission obtained when the secondary laser frequency ω' is scanned in the vicinity of comb line $\mu' = -3$. The trace contains features indicating the position of the microresonator resonance frequency $\omega_{-3}/(2\pi)$ and the soliton comb line frequency f_{-3} as well as the sideband injection locking range (see the main text for details). (b) Similar to (a) but for all μ' that can be reached by the scanning laser frequency ω'. In this representation, the resonance frequencies form a quadratic integrated dispersion profile (due to anomalous dispersion), while the equidistant soliton microcomb lines [highlighted in gray and expanded in panel (b)] form a straight line, enabling retrieval of pump laser detuning and microcomb repetition rate (see the main text for details). (c) Zoom into (b), focusing on the vicinity of the comb lines. The spectral dependence of the locking range can be observed [cf. panel (a) and see the main text for details]. (d) Locking range as a function of the relative mode number μ'. The measured data closely follow the predicted scaling (cf. the main text). The gray area indicates the uncertainty we expect from 10% detuning fluctuations during the recording procedure. (e) Locking range in terms of the repetition rate f_{rep} for $\mu' = -13$ as a function of secondary pump power (estimated on-chip power). Analogous to (d), the uncertainty is ∼±4%.

momentum is invariant under Kerr-nonlinear interaction (neglecting the Raman effect) and hence entirely defined by the driving lasers and the rate with which they inject photons of specific momentum into the cavity (balancing the cavity loss). If only the main pump laser is present, then $\bar{\mu} = 0$. However, in an injection-locked state, depending on phase, the secondary pump laser can coherently inject (extract) photons from the resonator, shifting $\bar{\mu}$ toward (away from) μ'. This is equivalent to a spectral translation of the intracavity field, consistent with the experimental evidence in Fig. 2(c).

To verify the validity of Eqs. (1) and (2), we perform a numerical simulation based on the Lugiato–Lefever equation (see Sec. IV of the supplementary material). We find excellent agreement between the analytic model and the simulated locking range. We note that Eqs. (1) and (2) are derived in the limit of low injection power, which we assume is the most relevant case. For a large injection power, the spectrum may shift substantially and consequently affect the values of P_μ. Interestingly, while this effect leads to an asymmetric locking range, the extent of the locking range is only weakly affected as long as the spectrum can locally be approximated by a linear function across a spectral width comparable to the shift. Injection into a sharp spectral feature (dispersive wave) is studied by Moille *et al.*[34]

The values of P_μ do not generally follow a simple analytic expression and can be influenced by the Raman effect and higher-order dispersion. While our derivation accounts for the values of P_μ [e.g., for the Raman effect, a_μ and P_μ are increased (reduced) for μ below (above) $\mu = 0$], it does not include a physical description for

Raman- or higher-order dispersion effects; these effects may further modify the locking range.

Taking into account the spectral envelope of the DKS pulse as well as the power of the injecting laser (which is not perfectly constant over its scan bandwidth), we fit the scaling $\delta_{\text{lock}} \propto \mu'^2 \sqrt{P' P_{\mu'}}$ to the measured locking range in Fig. 3(d), where we assume $P_{\mu'}$ to follow an offset (Raman-shifted) sech^2-function. The fit and the measured data are in excellent agreement, supporting our analysis and suggesting that the Raman shift does not significantly change the scaling behavior. Note that the effect of the last factor in Eq. (1) is marginal, and the asymmetry in the locking range is due to the impact of the Raman effect on P_μ. It is worth emphasizing that our analysis did not assume the intracavity waveform to be a DKS state and we expect that the analytic approach can, in principle, also be applied to other stable waveforms, including those in normal dispersion combs.[31,58] Indeed, as numerically shown in Sec. IV of the supplementary material, sideband-injection locking is also possible for normal dispersion combs. Here, in contrast to a DKS, sideband laser injection is found to have a strong impact on the spectral shape (not only the spectral shift). Therefore, although the underlying mechanism is the same as in DKS combs, Eqs. (1) and (2) do not generally apply (in the derivation, it is assumed that the spectrum does not change substantially).

Finally, as an example application of sideband injection locking, we demonstrate an optical frequency division, similar to previous work,[34] and measure the noise reduction in f_{rep} [Fig. 4(a)]. With a growing separation between the two driving lasers (increasing μ'), the phase noise is lowered by a factor of μ'^2, resulting in a phase noise reduction of more than three orders of magnitude (with respect to the free-running case) when injecting the secondary laser into the mode with index $\mu' = 42$ (limited by the tuning range of the secondary laser), and this without any form of stabilization of either the pump or the secondary laser. Figures 4(b) and 4(c) show the comparison of the repetition rate beatnote of the free-running and injection-locked cases.

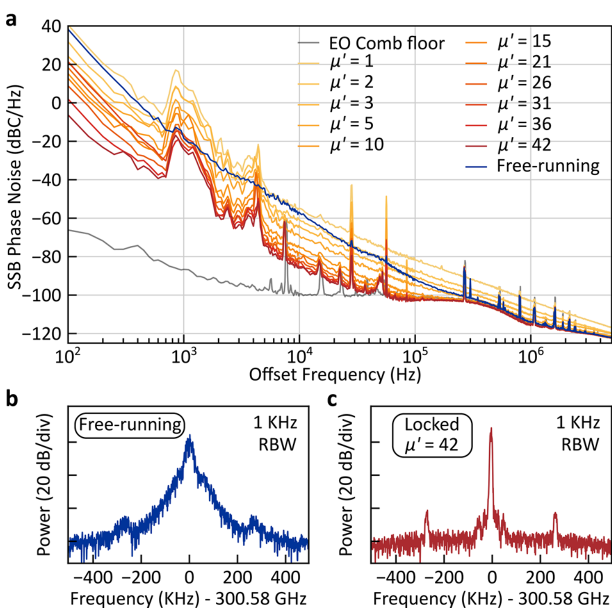

FIG. 4. Optical frequency division. (a) Repetition rate phase noise of the soliton microcomb in the free-running and locked states, with values of μ' ranging from 1 to 42. At higher offset frequencies (>100 kHz), the phase noise of the electro-optic modulation used to down-mix the 300 GHz repetition rate signal to detectable frequencies (see the supplementary material) limits the measurement. (b) Repetition rate beatnote recorded in the free-running state. (c) Repetition rate beatnote recorded in the locked state ($\mu' = 42$). The sidebands at ~±300 kHz are an artifact of the electro-optic modulation-based repetition rate detection scheme.

III. CONCLUSION

In conclusion, we have presented an experimental and analytic study of sideband injection locking in DKS microcombs. The presented results reveal the dependence of the locking range on the intracavity spectrum and on the injecting secondary laser, with excellent agreement between experiment and theory. While our experiments focus on the important class of DKS states, we emphasize that the theoretical framework from which we derive the presented scaling laws is not restricted to DKSs and may potentially be transferred to other stable waveforms. Our results provide a solid basis for the design of sideband injection-locked and parametrically generated Kerr-frequency combs and may, in the future, enable new approaches to low-noise microwave generation, compact optical clocks with simplified locking schemes, and, more generally, stabilized low-noise frequency comb sources from Kerr-nonlinear resonators.

SUPPLEMENTARY MATERIAL

See the supplementary material for more details on the experimental setup, the derivation of the locking range, the presentation of the numerical simulations, and considerations on thermal effects.

ACKNOWLEDGMENTS

This project has received funding from the European Research Council (ERC) under the EU's Horizon 2020 research and innovation program (Grant Agreement No. 853564) and through the Helmholtz Young Investigators Group VH-NG-1404; this work was supported through the Maxwell computational resources operated at DESY.

AUTHOR DECLARATIONS

Conflict of Interest

The authors have no conflicts to disclose.

Author Contributions

Thibault Wildi: Conceptualization (equal); Data curation (lead); Formal analysis (equal); Investigation (lead); Methodology (equal); Resources (equal); Software (lead); Validation (lead); Visualization (lead); Writing – original draft (equal); Writing – review & editing (equal). **Alexander Ulanov**: Methodology (equal); Resources (equal); Writing – original draft (supporting). **Nicolas Englebert**: Methodology (equal); Resources (equal); Writing – original draft (supporting). **Thibault Voumard**: Methodology (equal); Resources (equal). **Tobias Herr**: Conceptualization (equal); Formal analysis (equal); Funding acquisition (equal); Methodology (equal); Resources (equal); Supervision (equal); Writing – original draft (equal); Writing – review & editing (equal).

DATA AVAILABILITY

The data that support the findings of this study are available from the corresponding author upon reasonable request.

REFERENCES

[1] P. Del'Haye, A. Schliesser, O. Arcizet, T. Wilken, R. Holzwarth, and T. J. Kippenberg, "Optical frequency comb generation from a monolithic microresonator," Nature **450**, 1214–1217 (2007).
[2] T. J. Kippenberg, R. Holzwarth, and S. A. Diddams, "Microresonator-based optical frequency combs," Science **332**, 555–559 (2011).
[3] A. Pasquazi, M. Peccianti, L. Razzari, D. J. Moss, S. Coen, M. Erkintalo, Y. K. Chembo, T. Hansson, S. Wabnitz, P. Del'Haye, X. Xue, A. M. Weiner, and R. Morandotti, "Micro-combs: A novel generation of optical sources," Phys. Rep. **729**, 1–81 (2018).
[4] T. Fortier and E. Baumann, "20 years of developments in optical frequency comb technology and applications," Commun. Phys. **2**, 153 (2019).
[5] S. A. Diddams, K. Vahala, and T. Udem, "Optical frequency combs: Coherently uniting the electromagnetic spectrum," Science **369**, eaay3676 (2020).
[6] F. Leo, S. Coen, P. Kockaert, S.-P. Gorza, P. Emplit, and M. Haelterman, "Temporal cavity solitons in one-dimensional Kerr media as bits in an all-optical buffer," Nat. Photonics **4**, 471–476 (2010).
[7] T. Herr, V. Brasch, J. D. Jost, C. Y. Wang, N. M. Kondratiev, M. L. Gorodetsky, and T. J. Kippenberg, "Temporal solitons in optical microresonators," Nat. Photonics **8**, 145–152 (2014).
[8] T. Wildi, M. A. Gaafar, T. Voumard, M. Ludwig, and T. Herr, "Dissipative Kerr solitons in integrated Fabry–Perot microresonators," Optica **10**, 650–656 (2023).
[9] N. Lilienfein, C. Hofer, M. Högner, T. Saule, M. Trubetskov, V. Pervak, E. Fill, C. Riek, A. Leitenstorfer, J. Limpert, F. Krausz, and I. Pupeza, "Temporal solitons in free-space femtosecond enhancement cavities," Nat. Photonics **13**, 214–218 (2019).
[10] T. J. Kippenberg, A. L. Gaeta, M. Lipson, and M. L. Gorodetsky, "Dissipative Kerr solitons in optical microresonators," Science **361**, eaan8083 (2018).
[11] P. Marin-Palomo, J. N. Kemal, M. Karpov, A. Kordts, J. Pfeifle, M. H. P. Pfeiffer, P. Trocha, S. Wolf, V. Brasch, M. H. Anderson, R. Rosenberger, K. Vijayan, W. Freude, T. J. Kippenberg, and C. Koos, "Microresonator-based solitons for massively parallel coherent optical communications," Nature **546**, 274–279 (2017).
[12] A. A. Jørgensen, D. Kong, M. R. Henriksen, F. Klejs, Z. Ye, Ò. B. Helgason, H. E. Hansen, H. Hu, M. Yankov, S. Forchhammer, P. Andrekson, A. Larsson, M. Karlsson, J. Schröder, Y. Sasaki, K. Aikawa, J. W. Thomsen, T. Morioka, M. Galili, V. Torres-Company, and L. K. Oxenløwe, "Petabit-per-second data transmission using a chip-scale microcomb ring resonator source," Nat. Photonics **16**, 798–802 (2022).
[13] P. Trocha, M. Karpov, D. Ganin, M. H. P. Pfeiffer, A. Kordts, S. Wolf, J. Krockenberger, P. Marin-Palomo, C. Weimann, S. Randel, W. Freude, T. J. Kippenberg, and C. Koos, "Ultrafast optical ranging using microresonator soliton frequency combs," Science **359**, 887–891 (2018).
[14] M.-G. Suh and K. J. Vahala, "Soliton microcomb range measurement," Science **359**, 884–887 (2018).
[15] J. Riemensberger, A. Lukashchuk, M. Karpov, W. Weng, E. Lucas, J. Liu, and T. J. Kippenberg, "Massively parallel coherent laser ranging using a soliton microcomb," Nature **581**, 164–170 (2020).
[16] M.-G. Suh, X. Yi, Y.-H. Lai, S. Leifer, I. S. Grudinin, G. Vasisht, E. C. Martin, M. P. Fitzgerald, G. Doppmann, J. Wang, D. Mawet, S. B. Papp, S. A. Diddams, C. Beichman, and K. Vahala, "Searching for exoplanets using a microresonator astrocomb," Nat. Photonics **13**, 25 (2019).
[17] E. Obrzud, M. Rainer, A. Harutyunyan, M. H. Anderson, J. Liu, M. Geiselmann, B. Chazelas, S. Kundermann, S. Lecomte, M. Cecconi, A. Ghedina, E. Molinari, F. Pepe, F. Wildi, F. Bouchy, T. J. Kippenberg, and T. Herr, "A microphotonic astrocomb," Nat. Photonics **13**, 31 (2019).
[18] M.-G. Suh, Q.-F. Yang, K. Y. Yang, X. Yi, and K. J. Vahala, "Microresonator soliton dual-comb spectroscopy," Science **354**, 600–603 (2016).
[19] W. Liang, D. Eliyahu, V. S. Ilchenko, A. A. Savchenkov, A. B. Matsko, D. Seidel, and L. Maleki, "High spectral purity Kerr frequency comb radio frequency photonic oscillator," Nat. Commun. **6**, 7957 (2015).
[20] E. Lucas, P. Brochard, R. Bouchand, S. Schilt, T. Südmeyer, and T. J. Kippenberg, "Ultralow-noise photonic microwave synthesis using a soliton microcomb-based transfer oscillator," Nat. Commun. **11**, 374 (2020).
[21] J. Feldmann, N. Youngblood, M. Karpov, H. Gehring, X. Li, M. Stappers, M. Le Gallo, X. Fu, A. Lukashchuk, A. S. Raja, J. Liu, C. D. Wright, A. Sebastian, T. J. Kippenberg, W. H. P. Pernice, and H. Bhaskaran, "Parallel convolutional processing using an integrated photonic tensor core," Nature **589**, 52–58 (2021).
[22] H. Taheri, A. B. Matsko, and L. Maleki, "Optical lattice trap for Kerr solitons," Eur. Phys. J. D **71**, 153 (2017).
[23] Z. Lu, H.-J. Chen, W. Wang, L. Yao, Y. Wang, Y. Yu, B. E. Little, S. T. Chu, Q. Gong, W. Zhao, X. Yi, Y.-F. Xiao, and W. Zhang, "Synthesized soliton crystals," Nat. Commun. **12**, 3179 (2021).
[24] T. M. Fortier, M. S. Kirchner, F. Quinlan, J. Taylor, J. C. Bergquist, T. Rosenband, N. Lemke, A. Ludlow, Y. Jiang, C. W. Oates, and S. A. Diddams, "Generation of ultrastable microwaves via optical frequency division," Nat. Photonics **5**, 425–429 (2011).
[25] S. B. Papp, P. Del'Haye, and S. A. Diddams, "Parametric seeding of a microresonator optical frequency comb," Opt. Express **21**, 17615–17624 (2013).
[26] H. Taheri, A. A. Eftekhar, K. Wiesenfeld, and A. Adibi, "Soliton Formation in whispering-gallery-mode resonators via input phase modulation," IEEE Photonics J. **7**, 2200309 (2015).
[27] T. Hansson and S. Wabnitz, "Bichromatically pumped microresonator frequency combs," Phys. Rev. A **90**, 013811 (2014).
[28] J. K. Jang, M. Erkintalo, S. Coen, and S. G. Murdoch, "Temporal tweezing of light through the trapping and manipulation of temporal cavity solitons," Nat. Commun. **6**, 7370 (2015).
[29] M. Erkintalo, S. G. Murdoch, and S. Coen, "Phase and intensity control of dissipative Kerr cavity solitons," J. R. Soc. N. Z. **52**, 149–167 (2022).
[30] J. K. Jang, A. Klenner, X. Ji, Y. Okawachi, M. Lipson, and A. L. Gaeta, "Synchronization of coupled optical microresonators," Nat. Photonics **12**, 688–693 (2018).
[31] B. Y. Kim, J. K. Jang, Y. Okawachi, X. Ji, M. Lipson, and A. L. Gaeta, "Synchronization of nonsolitonic Kerr combs," Sci. Adv. **7**, eabi4362 (2021).
[32] H. Taheri, A. B. Matsko, L. Maleki, and K. Sacha, "All-optical dissipative discrete time crystals," Nat. Commun. **13**, 848 (2022).
[33] G. Moille, C. Menyuk, Y. K. Chembo, A. Dutt, and K. Srinivasan, "Synthetic frequency lattices from an integrated dispersive multi-color soliton," arXiv:2210.09036 [physics] (2022).
[34] G. Moille, J. Stone, M. Chojnacky, C. Menyuk, and K. Srinivasan, "Kerr-induced synchronization of a cavity soliton to an optical reference for integrated frequency comb clockworks," arXiv:2305.02825 [physics] (2023).
[35] P. Del'Haye *et al.*, "Self-injection locking and phase-locked states in microresonator-based optical frequency combs," Phys. Rev. Lett. **112**, 043905 (2014).
[36] H. Taheri, P. Del'Haye, A. A. Eftekhar, K. Wiesenfeld, and A. Adibi, "Self-synchronization phenomena in the Lugiato–Lefever equation," Phys. Rev. A **96**, 013828 (2017).
[37] Y. Wang, F. Leo, J. Fatome, M. Erkintalo, S. G. Murdoch, and S. Coen, "Universal mechanism for the binding of temporal cavity solitons," Optica **4**, 855–863 (2017).
[38] N. Englebert, C. Simon, C. M. Arabí, F. Leo, and S.-P. Gorza, "Cavity solitons formation above the fundamental limit imposed by the Raman self-frequency shift," in *CLEO 2023* (Optica Publishing Group, 2023), p. SW3G.3.

[39]H. Taheri, A. Savchenkov, and A. B. Matsko, "Stable Kerr frequency combs excited in the vicinity of strong modal dispersion disruptions," in *Laser Resonators, Microresonators, and Beam Control XXV* (SPIE, 2023), Vol. 12407, pp. 35–43.
[40]R. Suzuki, S. Fujii, A. Hori, and T. Tanabe, "Theoretical study on dual-comb generation and soliton trapping in a single microresonator with orthogonally polarized dual pumping," IEEE Photonics J. **11**, 6100511 (2019).
[41]Q.-F. Yang, X. Yi, K. Y. Yang, and K. Vahala, "Counter-propagating solitons in microresonators," Nat. Photonics **11**, 560–564 (2017).
[42]Q.-F. Yang, B. Shen, H. Wang, M. Tran, Z. Zhang, K. Y. Yang, L. Wu, C. Bao, J. Bowers, A. Yariv, and K. Vahala, "Vernier spectrometer using counterpropagating soliton microcombs," Science **363**, 965–968 (2019).
[43]Y. Wang, C. Yang, and C. Bao, "Vernier frequency locking in counterpropagating Kerr solitons," Phys. Rev. Appl. **20**, 014015 (2023).
[44]H. Taheri, A. B. Matsko, T. Herr, and K. Sacha, "Dissipative discrete time crystals in a pump-modulated Kerr microcavity," Commun. Phys. **5**, 159 (2022).
[45]E. Obrzud, S. Lecomte, and T. Herr, "Temporal solitons in microresonators driven by optical pulses," Nat. Photonics **11**, 600–607 (2017).
[46]M. H. Anderson, R. Bouchand, J. Liu, W. Weng, E. Obrzud, T. Herr, and T. J. Kippenberg, "Photonic chip-based resonant supercontinuum via pulse-driven Kerr microresonator solitons," Optica **8**, 771–779 (2021).
[47]W. Weng, E. Lucas, G. Lihachev, V. E. Lobanov, H. Guo, M. L. Gorodetsky, and T. J. Kippenberg, "Spectral purification of microwave signals with disciplined dissipative Kerr solitons," Phys. Rev. Lett. **122**, 013902 (2019).
[48]V. Brasch, E. Obrzud, S. Lecomte, and T. Herr, "Nonlinear filtering of an optical pulse train using dissipative Kerr solitons," Optica **6**, 1386 (2019).
[49]S.-P. Yu, D. C. Cole, H. Jung, G. T. Moille, K. Srinivasan, and S. B. Papp, "Spontaneous pulse formation in edgeless photonic crystal resonators," Nat. Photonics **15**, 461–467 (2021).
[50]A. E. Ulanov, T. Wildi, N. G. Pavlov, J. D. Jost, M. Karpov, and T. Herr, "Synthetic-reflection self-injection-locked microcombs," arXiv:2301.13132 [physics] (2023).
[51]M. Karpov, H. Guo, A. Kordts, V. Brasch, M. H. P. Pfeiffer, M. Zervas, M. Geiselmann, and T. J. Kippenberg, "Raman self-frequency shift of dissipative Kerr solitons in an optical microresonator," Phys. Rev. Lett. **116**, 103902 (2016).
[52]X. Yi, Q.-F. Yang, K. Y. Yang, and K. Vahala, "Theory and measurement of the soliton self-frequency shift and efficiency in optical microcavities," Opt. Lett. **41**, 3419 (2016).
[53]R. Adler, "A study of locking phenomena in oscillators," Proc. IRE **34**, 351–357 (1946).
[54]P. Del'Haye, O. Arcizet, M. L. Gorodetsky, R. Holzwarth, and T. J. Kippenberg, "Frequency comb assisted diode laser spectroscopy for measurement of microcavity dispersion," Nat. Photonics **3**, 529–533 (2009).
[55]A. B. Matsko and L. Maleki, "Feshbach resonances in Kerr frequency combs," Phys. Rev. A **91**, 013831 (2015).
[56]E. Lucas, M. Karpov, H. Guo, M. L. Gorodetsky, and T. J. Kippenberg, "Breathing dissipative solitons in optical microresonators," Nat. Commun. **8**, 736 (2017).
[57]G. Hadley, "Injection locking of diode lasers," IEEE J. Quantum Electron. **22**, 419–426 (1986).
[58]X. Xue, M. Qi, and A. M. Weiner, "Normal-dispersion microresonator Kerr frequency combs," Nanophotonics **5**, 244–262 (2016).